Challenges in inferring breathing rhythms from olfactory bulb local field potentials

Sidney E. Rafilson[1,2,4], Nathan Hess[3], Teresa M. Findley[1], Matthew C. Smear[1,3]

[1]Institute of Neuroscience, University of Oregon, Eugene Oregon, United States

[2]Department of Mathematics, University of Oregon, Eugene Oregon, United States

[3]Department of Psychology, University of Oregon, Eugene Oregon, United States

[4]Department of Biology, University of Oregon, Eugene Oregon, United States

Author for correspondence: Matthew C. Smear (smear@uoregon.edu)

Abstract

Odors convey useful navigational and episodic information, yet much of the chemical world remains inaccessible without active sampling through sniffing. To effectively interpret olfactory cues, the brain must unify odor-driven activity with respiratory cycles, making accurate respiratory measurements critical in understanding olfactory bulb (OB) dynamics. Previous studies have shown that behavioral signals are often present in primary sensory areas, and OB local field potentials (LFPs) have long been known to couple with respiration. Here we investigated whether OB LFPs can reliably recover the precise timing and frequency of respiration. Our results indicate that OB LFPs across multiple frequency bands align with respiratory cycles. Using time and frequency domain methods, we show that 2-12 Hz LFP oscillations effectively track respiratory frequency. However, a monotonic relationship between LFP-respiratory delay and sniffing frequency, which varies across animals, renders the recovery of precise respiratory events challenging. This work demonstrates the complex and individualized relationship between rodent respiration and OB LFPs, contributing to our understanding of how respiratory signals are represented in the OB.

Keywords: olfactory bulb local field potentials, active sampling, sniffing

Introduction

Sensation in the rodent olfactory system is modulated by respiratory behavior throughout the brain (Wachowiak et al., 2011). Beginning with inhalation, which drives the binding of odorants with olfactory sensory neurons (OSNs) (Kleene, 2008), the respiratory cycle further organizes downstream spiking activity. High-frequency respiration, or sniffing, modulates the temporal dynamics of the spatial map of odor identity at the olfactory sensory input, the glomerular layer (Spors et al., 2006; Verhagen et al., 2007). While odorants can be decoded from the spatial activity of glomeruli in the OB, this spatial representation is not chemotopic in the first order projection neurons, mitral and tufted (M/T) cells (Gupta, Albeanu, & Bhalla, 2014), except at near-threshold concentrations (Burton et al., 2022). In addition to this spatial coding, M/T cells seem to be dynamically tuned to timing in the respiratory cycle (Macrides and Chorover, 1972; Cury & Uchida, 2010), and to sniff frequencies (Sterrett et al., 2024); and this temporal encoding seems to be modulated by odor identity (Iwata, Kiyonari, and Imai, 2017), behavioral state, and external context (Sterrett et al., 2024). Because of the respiratory alignment of OB population dynamics, analyzing sniff-centric spiking activity has become a powerful tool for understanding the encoding of odor identity, concentration, and perceptual strength (Cury & Uchida, 2010; Wilson et al., 2017), as well as the effects of behavioral state and context on sensation (Sterrett et al., 2024).

Concurrent with the fast activity of single unit firing are slower voltage fluctuations known as local field potentials (LFPs). LFPs represent the sum of sub-threshold electrical activity; while the high frequency spiking activity is indicative of action potentials, the low frequency LFPs are thought to be a measure of collective neural activity, particularly synaptic activity (Buzsaki, Anastassiou & Koch, 2012). Despite measuring a fundamentally different aspect of OB activity, LFPs are coupled with respiratory behavior across multiple frequency bands and relate dynamically to odor learning, sensitization, and discrimination (Kay et al., 2009).

Low-frequency electrical oscillations in the OB, such as those observed in the theta band (1-15Hz), have been shown to align closely with rodent sniffing behavior. Specifically, theta oscillations are entrained by the respiratory rhythm, reflecting the synchronization of neural activity with the sniff cycle (Rojas-Libano et al., 2014). Additionally, higher frequency beta oscillations (15 - 30 Hz) also align with inhalation and have been implicated in driving hippocampal oscillations, suggesting a broader network synchronization during olfactory processing (Fourcaud-Trocmé et al., 2019; Lockmann et al., 2017). The highest frequency OB LFPs, gamma oscillations (65-85 Hz), are dynamically related to olfactory signal transduction, being evoked by sensory stimulation and enhanced during odor discrimination tasks (Kay et al., 2009). Gamma oscillations are thought to play a critical role in the processing and integration of olfactory information, particularly under high task demands (Beshel, Kopell & Kay, 2007; Lasacco et al., 2020). As with population dynamics, the synaptic activity measured by LFPs highlights the complex and dynamic synchrony of OB activity with respiration and odor dynamics (Cleland and Borthakur, 2020; Kay, Lancaster, and Freeman, 1996)

As in the analysis of spiking activity, accurately measuring respiratory events and frequency and aligning LFPs to inhalation onset is essential for understanding the collective neural activity in the OB (Rinberg, Koulakov, Gelperin, 2006; Shusterman et al., 2011). Despite numerous

methods of measuring respiration in rodents, each has its drawbacks, often leading to signal loss or contamination by noise.

Pressure sensor-coupled chambers for plethysmography provide precise measures of respiration but require a small recording chamber, which restricts animal mobility (Lim, 2014). Intranasal pressure or temperature sensors can solve the problem of animal mobility while maintaining high signal fidelity (Grimaud & Murthy, 2018); however, implanted sensors are surgically invasive, particularly around the OSNs, and prone to blockage (McAfee et al., 2016). Electromyograms of the diaphragm measures respiration without the drawback of blockage or injury to the nasal epithelium, but are extremely invasive (Grimaud & Murphy, 2018),

To address the issues of invasiveness and mobility while maintaining high signal fidelity, a method involving a chronically implanted temperature sensor, or thermistor, was devised. The thermistor is implanted into the hollow space above the anterior portion of the nasal cavity, safely avoiding the epithelium and nasal passages while still capturing respiration-driven temperature fluctuations (McAfee et al., 2016). While the thermistor provides a high-fidelity recording in mobile animals and minimizes invasiveness, the method still requires a craniotomy, and it suffers from signal degradation in recordings spanning weeks or months.

LFPs are often recorded in electrophysiological research of the olfactory system. To rigorously analyze OB population dynamics, understanding the timing and frequency of sniffing behavior is crucial. Considering the close alignment between OB LFPs and respiration, and given the difficulties in directly measuring sniffing behavior, we sought to determine whether a model could translate LFPs into sniffing parameters, such as inhalation onset and sniff frequency. In doing so, sniff-centric neural data could be studied without the need for direct respiratory measurement, but rather through a respiratory reconstruction from OB LFPs. We hypothesized that LFPs recorded from the OB faithfully recapitulate the timing and frequency of respiration in the freely moving mouse.

Materials and Methods

Animal housing and care

All procedures were conducted in accordance with the ethical guidelines of the National Institutes of Health and were approved by the Institutional Animal Care and Use Committee at the University of Oregon. Animals were maintained on a reverse 12/12 h light/dark cycle. All recordings were performed during the dark phase of the cycle. Mice were C57Bl6/J background and were 8–12 weeks of age at the time of surgery.

Surgical procedures

Animals were anesthetized with isoflurane (3% concentration initially, altered during surgery depending on response of the animal to anesthesia). Incision sites were numbed prior to incision with 20 mg/mL lidocaine.

Thermistors were implanted between the nasal bone and inner nasal epithelium (Findley et al., 2021). A custom titanium head bar and Janelia micro drive were implanted.

For olfactory bulb array implantation, we administered atropine (0.03 mg/kg) preoperatively to reduce inflammation and respiratory irregularities. Surgical anesthesia was induced and maintained with isoflurane (1.25–2.0%). Skin overlying the skull between the lambdoid and frontonasal sutures was removed. A rectangular window was cut through the skull overlying the lateral half of the left bulb for insertion of the recording array. The array was lowered to a depth of 1mm and cemented in place with Grip Cement. To minimize postoperative discomfort, Carpofen (10 mg/kg) was administered 45 minutes prior to the end of surgery. Mice were housed individually after the surgery and allowed 7 days of post-operative recovery.

Behavioral recordings

Mice were restrained by head fixation then placed in a 15 cm by 40cm behavioral arena. After a period of head-fixation, mice were released and permitted to freely move around the arena, without explicit training or reward structure, while breathing and neural data was collected.

We record sniffing using intranasally implanted thermistors (TE Sensor Solutions, #GAG22K7MCD419), amplified initially with custom-built op amp (Texas Instruments, #TLV2460, circuit available upon request) and then a CYGNAS, FLA 01 amplifier fed into the analog input of an OpenEphys box.

Electrophysiology

Following 3-day recovery period post-surgery mice were head fixed and the custom microdrive was advanced to the regions of interest (ROI) while recording. Either Si probes (PART NUMBER) or a custom implanted array of 8 tetrodes passed in pairs through 4 linearly-aligned 27-gauge stainless steel hypodermic tubes. Tetrodes were made of 18 μm (25 μm coated) tungsten wire (California Fine Wire). Once the ROI was reached a minimum of 24 hours was allowed prior to data collection to increase recording stability.

Data were acquired via a 128-channel data acquisition system (RHD2000; Intan Technologies) at a 30 kHz sampling frequency and OpenEphys software (http://open-ephys.org).

Custom Bonsai code was used to align the respiratory and the electrophysiology recording captured with no filters applied in the OpenEphys software.

Data Analysis

All data was analyzed in custom python scripts (Smear-Lab/sniff-LFP: Local Field Potential Project-- Smear Lab). LFP and thermistor preprocessing for all analysis consisted of lowpass filtering the signal below 300Hz using an order 4 Butterworth filter, followed by down sampling to 1 kHz, using the SciPy signal processing library. Inhalation times were extracted by finding peaks in the temperature signal after smoothing with a 25ms moving Savitsky-Golay filter. Sniffs with a duration less than the 5th and greater than the 95th percentile were excluded from the analysis.

Spectral Analysis

Power spectrum, spectral coherence and phase-shift were estimated between individual channels of the LFP and the thermistor signal.

To build time-frequency spectrograms, we used 90% overlapping 4s windows. This choice of window lengths yielded a lower bound on frequency content at 0.25 Hz and given the sampling rate, a Nyquist frequency of 500Hz. To home in on the frequency band of interest, we bandpass filtered the LFPs using another order 4 Butterworth filter. To limit spectral leakage in the short windows, the power spectrum estimates were computed using Thompsons Multitaper procedure (Thompson 1962). This method involves defining a time-bandwidth product NW where N is the window length and W is the half-bandwidth of interest. Then, K orthogonal data tapers from the Slepian sequence (Slepian, 1978) are computed for each window. Typically, $K \approx 2NW - 1$ and hence we chose to use 7 tapers. Finally, averaging the Fourier transforms of the time series by each of these tapers gives the final spectral estimate for the nth window:

$$S_n(f) = \frac{1}{K}\sum_{k=1}^{K}\left|X_{n,k}(f)\right|^2$$

Where $X_{n,k}(f)$ is the Fourier transform for the nth window and k^{th} taper such that

$$X_{n,k}(f) = \int_{-\infty}^{\infty} x_{n,k} \cdot v_k(t) \cdot e^{-i2\pi f t} dt$$

With $x_{n,k}(t)$ the signal in the nth window and $v_k(t)$ the kth data taper. Spectral coherence was calculated as follows:

$$C(f) = \frac{S_n^{12}(f)}{\sqrt{S_n^1(f) \cdot S_n^2(f)}}$$

Where $S_n^{12}(f)$ corresponds to the estimated cross-spectrum calculated by multiplying the spectral estimate of the first signal $S_n^1(f)$ with the complex conjugate of the spectral estimate of the second signal $\hat{S}_n^2$.

Time-frequency heatmaps represent coherence or spectral power by color with a linear color mapping fit to the middle 90% of the data range. Confidence limits on coherence were created by circularly shifting the thermistor signal before computing the windowed coherence. At least 1000 pseudo-random circular shifts were performed and a z-score threshold of 1.65 from the null coherence distribution was used as a lower limit on significant coherence.

Time-domain Analysis

In the time-domain we analyzed wavelengths and latencies between inhalation times and peaks in the LFPs. To reliably detect peaks, we averaged unit variance scaled LFP epochs aligned to inhalation times, within sniff frequency bins. The bins were linearly spaced between 2 and 12Hz with a width of 0.5Hz, thus discretizing the sniffing frequencies into 20 partitions. We detected peaks in the averaged LFP epochs using the SciPy find_peaks function with prominence of 0.1 and a minimum distance set to the reciprocal of the upper passband. This method allowed us to estimate the distributions of mean inhalation-to-peak latencies and LFP wavelengths across sniff frequencies, mice, and sessions.

Respiratory frequency inference

We inferred the average sniff frequency in sliding windows ranging from 1 to 128 seconds using time and frequency domain approaches. In both methods, we worked with the 2 – 12Hz bandpass filtered LFPs. In the time domain we took the mean reciprocal of the inter-peak-intervals. We infer the frequency of the wth window in the time domain by,

$$f_w^1 := \frac{1}{N_w - 1} \sum_{n=1}^{N_w - 1} \frac{1}{P_{n+1} - P_n}$$

Where P_n is the time of the nth peak and N_w the number of peaks in the associated window. The frequency domain method finds the frequency component of the power spectrum between 2 and 12 Hz with the maximum power. That is,

$$f_w^2 := arg\,\max_f S_w(f) : 2 \leq f \leq 12$$

Where S_w is the power spectrum in the associated window.

Results

Given the importance of respiration and the challenges of capturing it directly, we attempted to reconstruct respiration from OB LFPs in the frequency and time domains. To determine the spectral relationships between respiration and OB LFPs, we estimate PSDs and spectral coherence. First, time-frequency spectrograms show that the PSD of raw LFPs track instantaneous sniffing frequency (Figure 1; A). Validating our measure of instantaneous sniffing frequency, we built time-frequency spectrograms of the thermistor sniff signal and show that the power tracks the instantaneous sniff frequency (Figure 1; A). Taking the linear correlation between the two power spectra, we show that there is significant spectral coherence between raw LFPs and the thermistor sniff signal (Figure 1; B), and coherence tracks the instantaneous sniffing frequency (Figure 1; A, B, C). Further, the coherence reaches significance with respect to a null distribution in a narrow window associated with the instantaneous sniff frequency spectrum (Figure 1; B, C). We call this interval of significant coherence (2 – 12Hz) the theta band. These results reproduce previous studies showing that the low frequency LFP theta oscillations track breathing rhythms (Rojas-Libano et al., 2014).

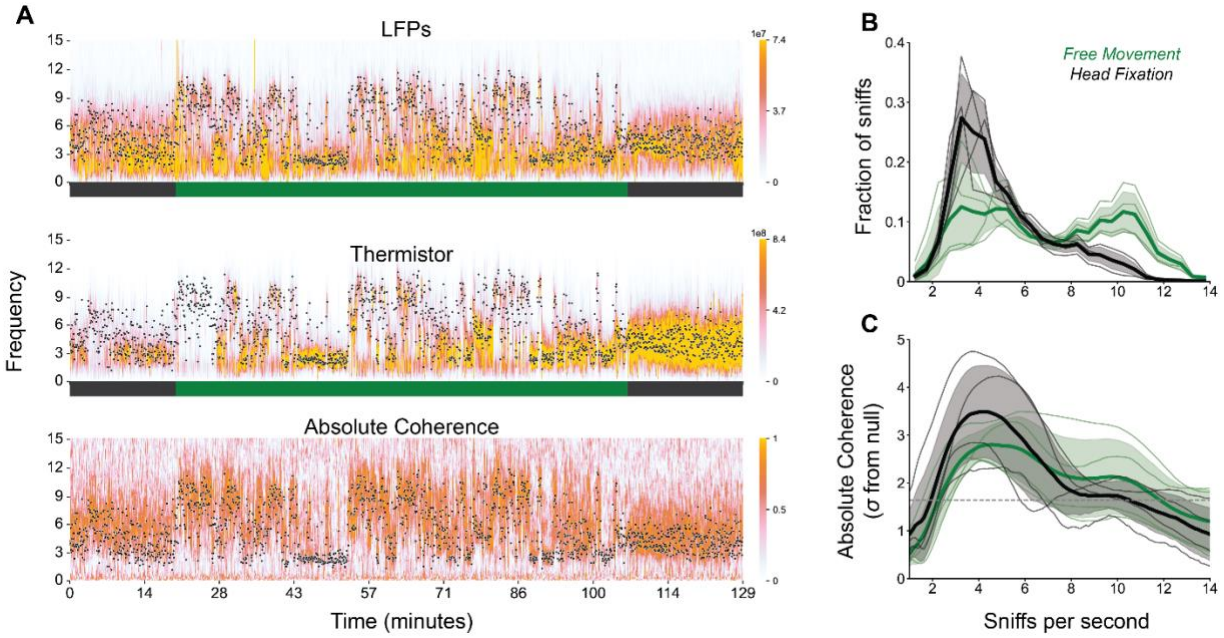

Figure 1: Spectral analysis reveals coherence between LFP and sniff signal. **A)** Spectrograms were computed using Thompson's multitaper method using five tapers in 4s windows sliding in 400ms increments. Black scatter overlay represents instantaneous sniff frequencies. For visual clarity, only a subset of instantaneous frequency points are plotted in the LFP and coherence plots. The color bar shows head fixation in black and free moving in green. Example session is shown ***Top***) Power spectral density (PSD) of raw LFPs. ***Middle***) PSD of thermistor signal. ***Bottom***) Absolute spectral coherence between LFP and thermistor signals. **B)** Instantaneous sniffing frequency distributions. **C)** Absolute spectral coherence between LFPs and thermistor sniff signal plotted as standard deviations from a null distribution. A dotted line represents z-score estimated 95% significance threshold. In both **B** and **C**: Thin lines represent individual mice with the thicker line to represent the grand mean. Shaded region is 1 standard deviation from the grand mean computed across mice. Color shows head fixation in black and free movement in green.

To explore the relationship between OB LFPs and respiration in the time domain, we constructed LFP epochs centered on inhalation onset and examined the time course of various features across the epochs. Raw LFPs align to inhalation onset via a constant delay to the first prominent peak. Further, the wavelength between successive prominent peaks correlates with respiratory cycle length (Figure 2). Bandpass filtering between 2 and 12Hz shows that the unfiltered LFP-respiratory relationship reflects this frequency range. We also found that 25 - 45Hz (beta) oscillations seem to be aligned by a latency to peak and wavelength invariant of sniff frequency (Figure 2). Finally, we bandpass filtered the LFPs between 65 and 85 Hz and aligned the amplitude envelope of these gamma oscillations to inhalation onset, finding similar alignment as in the theta band (Figure 2). We noticed no observable differences in latency to peak or LFP wavelength between free movement and head fixation. These visualizations reveal a robust time-domain alignment of LFPs in multiple frequency bands with respiration.

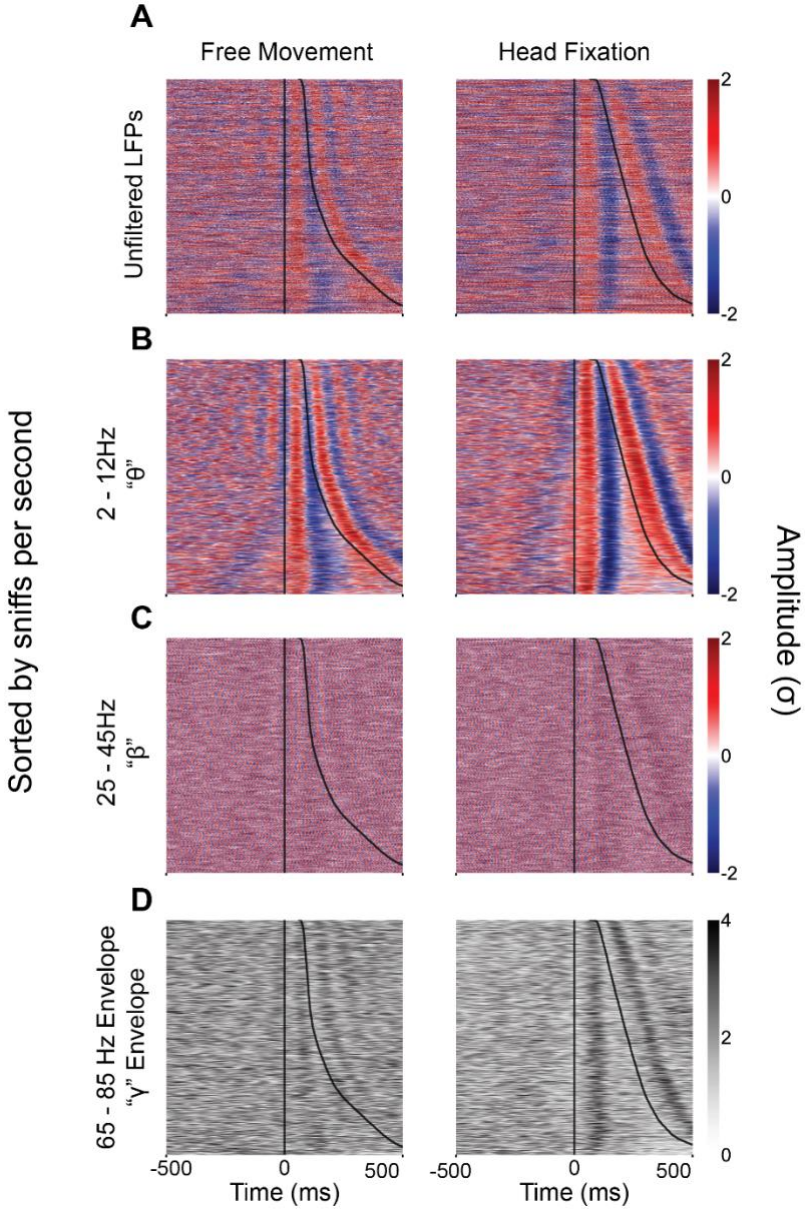

Figure 2: Time-domain visualizations from a representative session reveal OB LFPs in multiple frequency bands align to inhalation onset. Heatmaps show inhalation time aligned LFP epochs stacked in the y-direction according to the instantaneous sniffing frequency from which they are aligned. Each row represents an inhalation aligned LFP epoch with color to represents the amplitude of the unit variance scaled epoch. The vertical black line represents the inhalation time from which the epochs are aligned, and the sloped line represents the next inhalation time. **A)** Unfiltered, **B)** 2 – 12Hz 'theta', **C)** 25 – 45Hz 'beta', **D)** and the amplitude envelope of the 65 – 85Hz 'gamma envelope' LFPs are shown.

To rigorously analyze the relationship between LFPs and respiration in the time-domain, we sought to construct distributions of the delay to the first prominent peak and LFP inter-peak-interval, across the inhalation aligned epochs. We found that on a sniff-by-sniff basis, across all frequency bands, there were variable number of peaks per respiratory cycle. Because of this variance, understanding the distributions of delays and cycle lengths was challenging. While the visualizations indicate a systematic timing relationship between the LFP epochs and respiration, the variance in the number of prominent peaks per respiratory cycle suggests that this relationship may not be robust on a sniff-by-sniff basis.

To uncover time-domain relationships which may be masked by noise on a sniff-by-sniff basis, we averaged the unit variance scaled LFP epochs aligned to inhalation times, within sniff frequency bins, and detected peaks on these averaged LFP epochs. This method allowed us to analyze the mean normalized LFP epochs, which reliably contained fixed numbers of peaks per respiratory cycle. The mean theta band and gamma amplitude envelope epochs contained a single peak per respiratory cycle in over 98% of instances, whereas the beta band still contained variable number of peaks.

Using these averaged and normalized epochs, we found a strong linear correlation between respiratory and LFP cycle lengths in the theta band and gamma envelope oscillations during free movement and head fixation in all mice (Figure 3). We also found a non-linear monotonic relationship between respiratory cycle length and latency to peak in the theta band and gamma envelope (Figure 3). Further, mean latencies to LFP peak differed across mice, and in some sessions (Figure 4). In contrast, we found no association between the beta band cycle length or latency to LFP peak with respiratory cycle length (Figure 3).

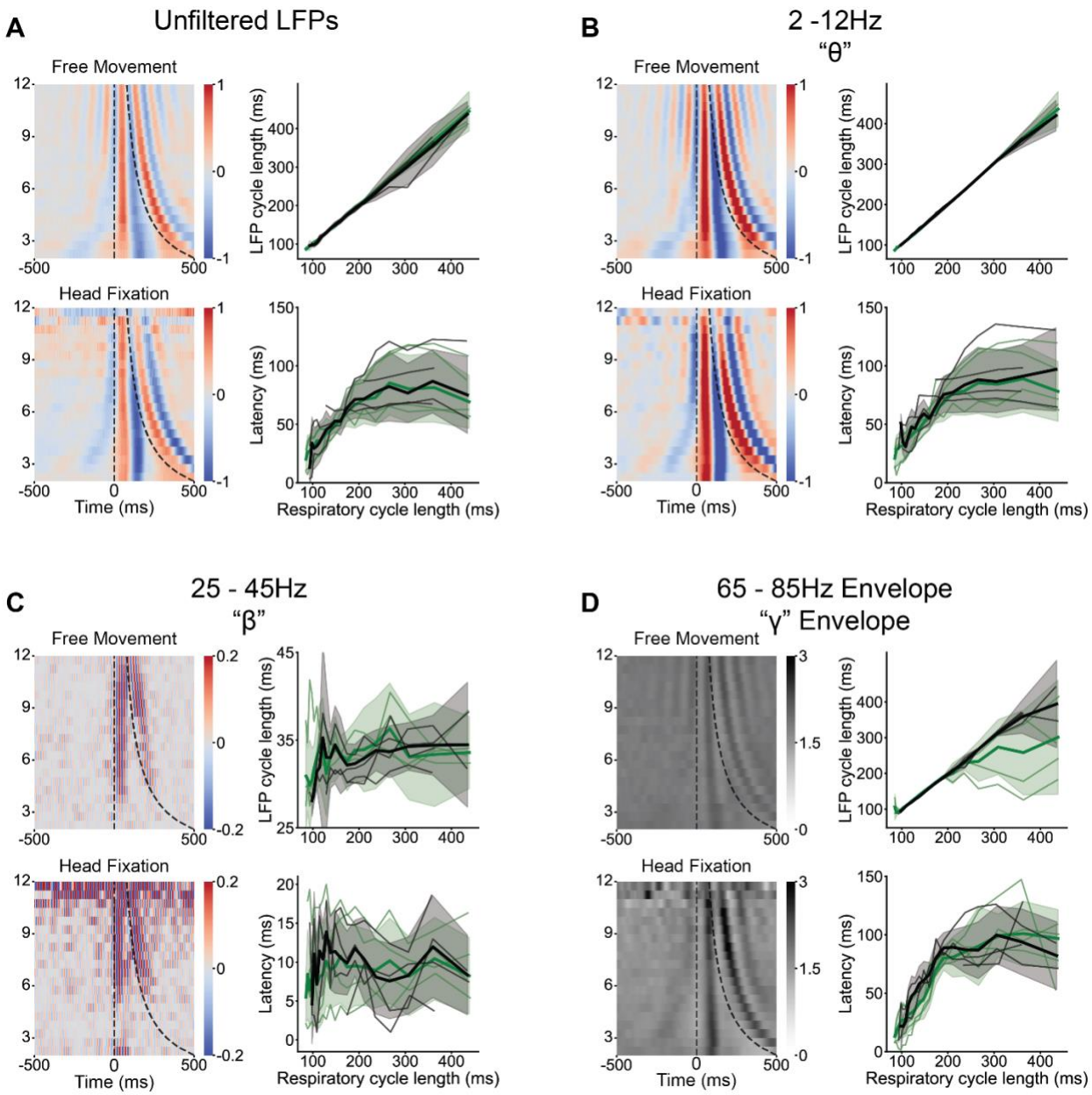

Figure 3: Averaging inhalation aligned LFP epochs within sniff frequency bins demonstrates timing relationships between LFPs and respiration. A) Unfiltered LFPs cycle lengths are linearly correlated with respiration cycle length and the delay to peaks is non-linearly correlated to cycle length. **B)** 2 – 12Hz oscillations show the same time-domain characteristics as raw LFPs with respect to respiration, but with a stronger correlation. **C)** 25 – 45Hz cycle lengths and latency to peak are invariant to respiratory cycle length. **D)** 65 – 85Hz envelope oscillations showed similar time-alignments to respiration as in the theta band, although with a stronger cycle length correlation in head fixed compared to free moving.

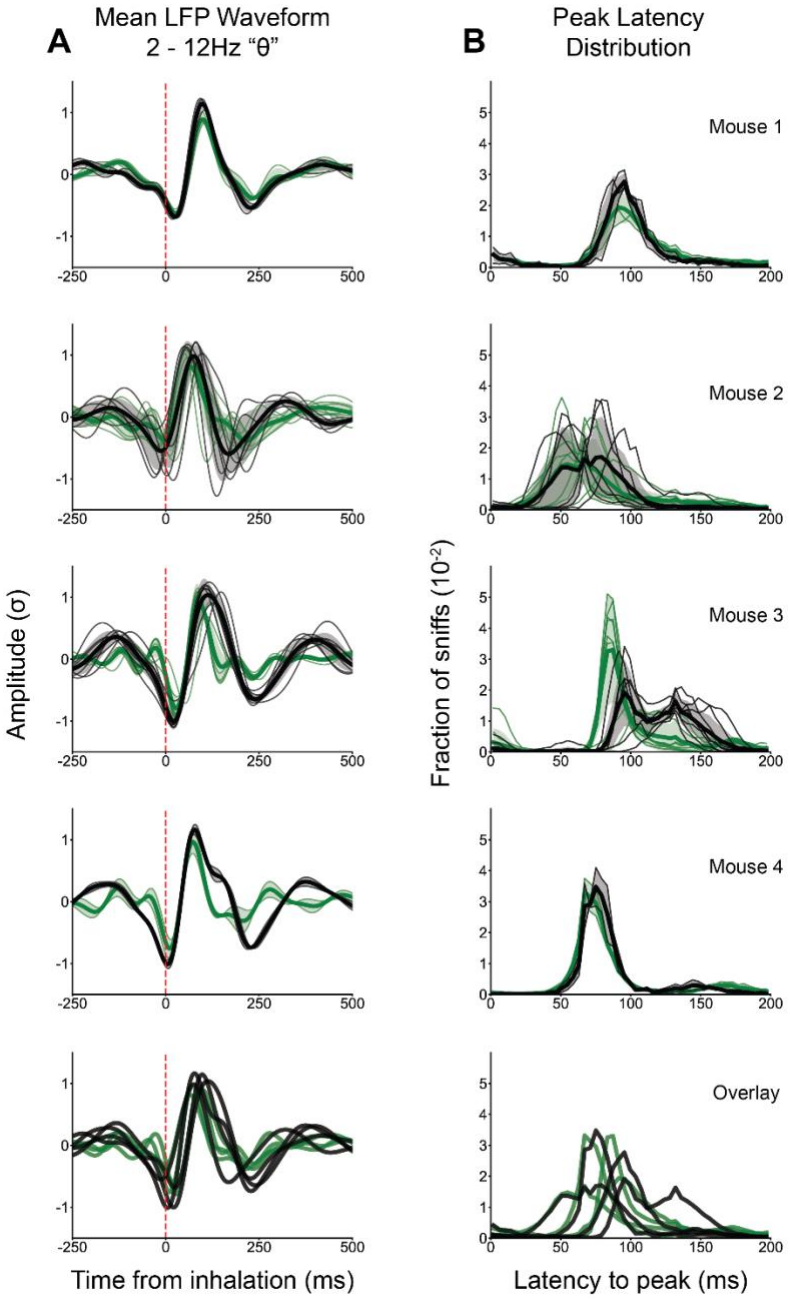

Figure 4: Local field potential peaks vary across mice in latency from inhalation. Mean waveform of the unit variance scaled 2 – 12 Hz 'theta' oscillations aligned to inhalation onset **A)** and the distribution of latencies to the peak in the LFPs **B)**. Each of the four mice are shown with thin lines to represent the sessions mean waveform and latency distribution. Overlay shows the mouse means. Head fixation represented in black with free movement in green. The peak latency distributions were constructed on a sniff-by-sniff basis by finding the distance between inhalation onset and the first prominent LFP peak. Distributions differ significantly across mice by two-sample Kolmogorov Smirnov test. In mouse 2 and 3, session distributions differ significantly.

Because of the spectral coherence and time-domain relationships between LFP and sniffing we asked if the precise timing of inhalation and the respiratory frequency could be inferred from the LFPs. The across-mouse variation in the mean latency from inhalation onset to peak in the LFPs and the LFP phase at inhalation onset renders recovering the precise timing of inhalation onset non-generalizable across mouse (Figure 4). However, the strong correlation between LFP and respiratory cycle length suggests that the respiratory frequency can be recovered from the 2 – 12Hz LFPs. To test this hypothesis, we devised time and frequency domain methods of inferring respiratory frequency using sliding windows of LFP. The time-domain method finds the mean inter-peak-interval in the LFP window whereas and a frequency domain method estimates

the frequency with maximum power. We found that time-domain method outperformed the frequency method and both models performed better during free movement compared to head fixation. Notably, during free movement using the time-domain method we can infer sniffing frequency within 1Hz in over 75% of windows ($\sigma < 1$) when the window size is at least 8 seconds (Figure 5). We also noticed that pervasive low frequency power is responsible for the inferiority of the frequency-domain method (Figure 6).

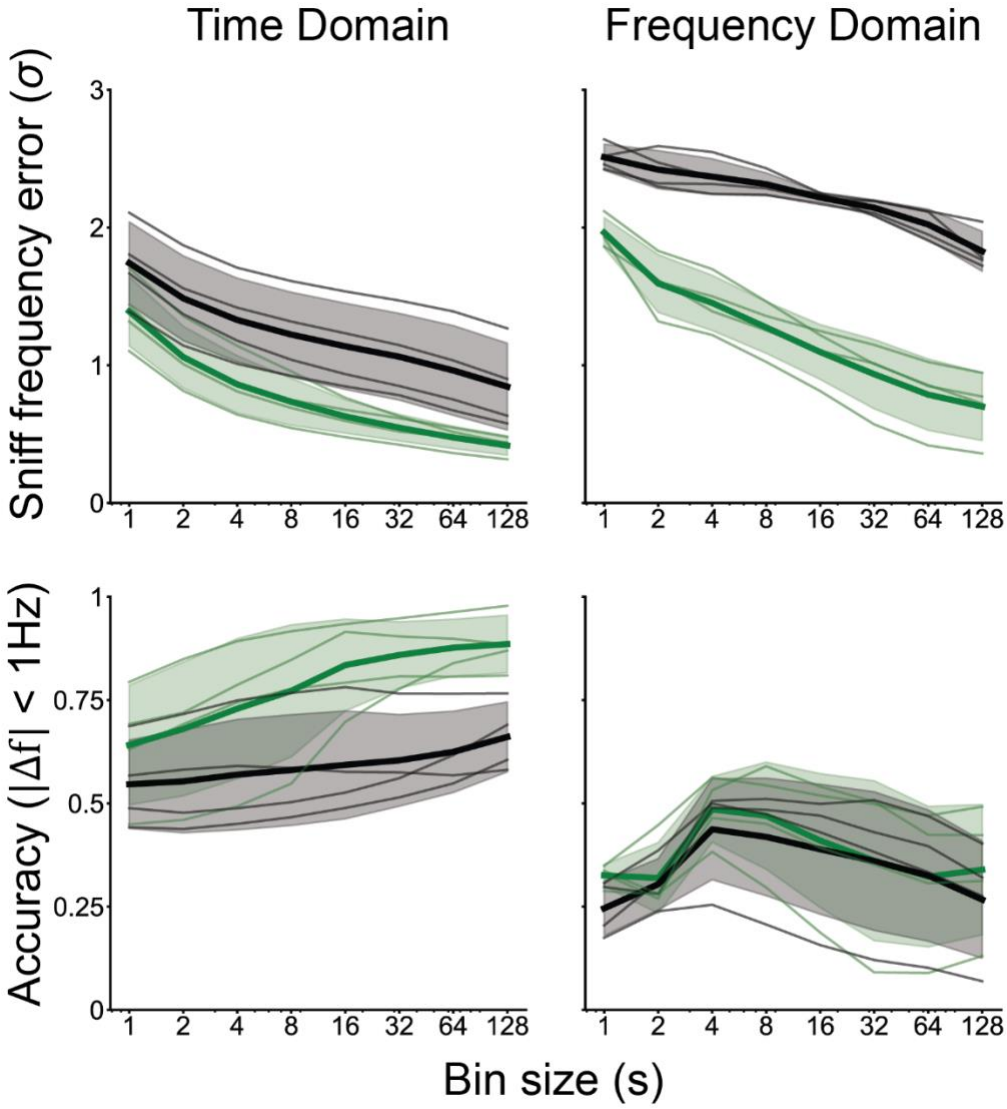

Figure 5: Respiratory frequency in sliding windows can be recovered from LFPs. Time domain method uses the mean reciprocal of inter-peak-intervals. Frequency domain method uses the maximum in the power spectrum. Both methods are applied in sliding windows of variable size with 50% overlap. The prediction error is represented as the standard deviation in Hz of true vs inferred sniff frequencies and the accuracy is defined as inferred frequencies which are within 1Hz of the true value. Thin lines represent individual mice across all sessions with thicker lines to represent the grand mean. Head fixation is in black and free movement is in green.

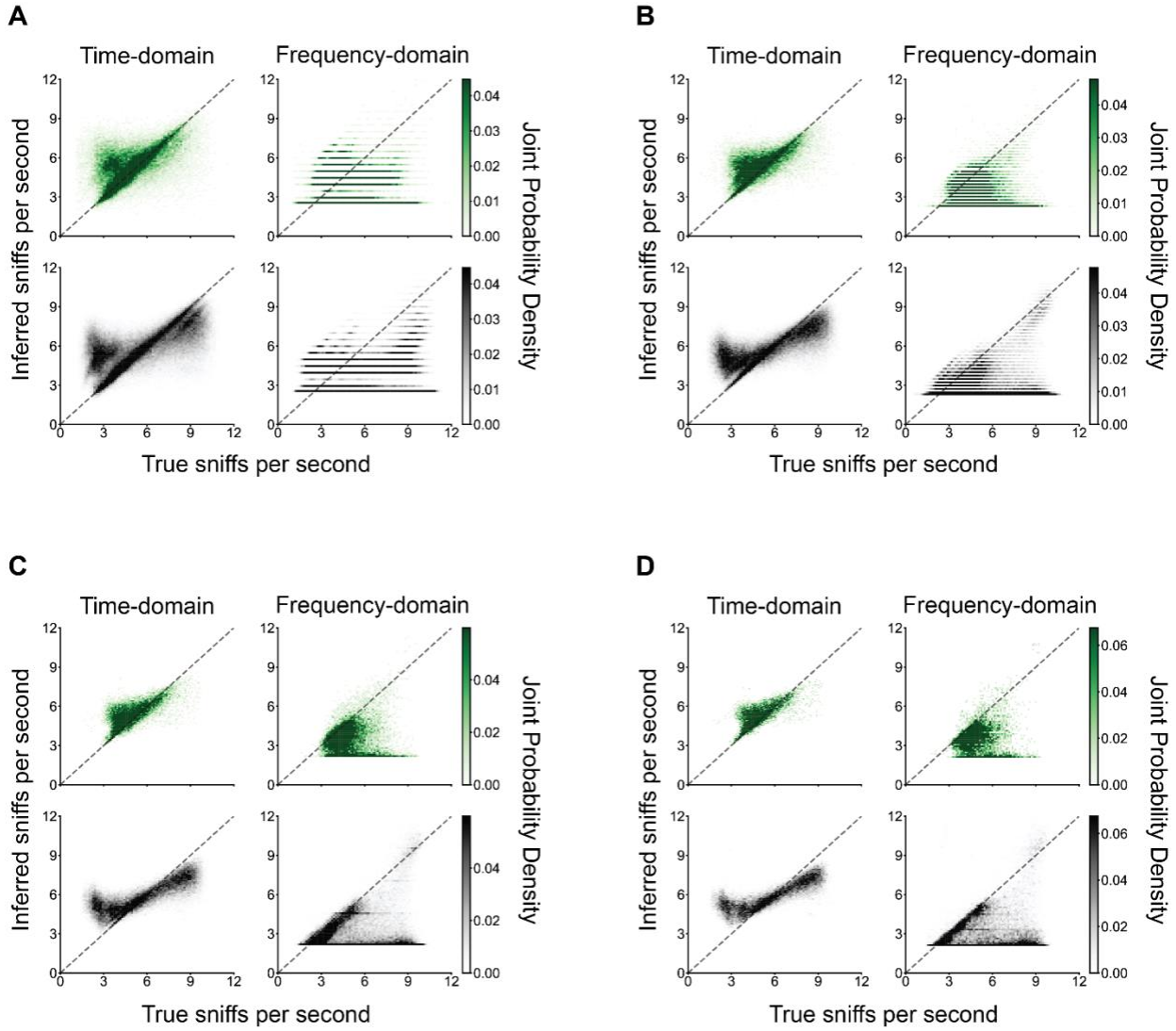

Figure 6: Heatmap shows the joint probability density of inferred vs true respiratory frequencies in 1, 2, 4 and 8 second sliding windows (**A**, **B**, **C**, **D**, respectively). Colormaps fit to the lower 95% of the density. Head fixation is represented in black and free movement is represented in green.

Discussion

Inferring precise respiratory dynamics from OB LFPs presents several challenges despite their clear respiratory coupling. Our study demonstrated strong coherence between OB LFPs and respiration, particularly in the 2-12 Hz theta band, which has previously been shown to track the respiratory cycle (Rojas-Libano et al., 2014). However, recovering the exact timing of inhalation onset and sniff frequency based on LFPs proved more difficult due to variability in the latency of LFP peaks and inconsistencies across sniff cycles and individual animals.

One of the primary challenges arises from the inherent variability in the number of LFP peaks per respiratory cycle. While theta band oscillations often show alignment to the sniff cycle, the delay between inhalation onset and LFP peaks is not consistent across cycles. This variability complicates the inference of precise timing for respiratory events. Our results show that while averaged LFP epochs reliably contain a single peak per respiratory cycle, the timing of these peaks relative to inhalation onset varies across individual sniffs and mice. This observation suggests that while LFPs may broadly represent respiratory rhythms, the exact timing of respiratory events such as inhalation onset may be masked by inter-trial and inter-subject variability.

This variability is likely due to the complex, multi-frequency composition of the OB LFP signal, as different oscillatory bands (theta, beta, gamma) exhibit distinct relationships with respiration. 2-12 Hz theta oscillations exhibited the strongest correlation with respiratory frequency (Rojas-Libano et al., 2014), but higher frequency oscillations, such as the 25-45 Hz beta and 65-85 Hz gamma envelope oscillations, showed less consistent alignment with respiration. The beta band did not demonstrate a clear correlation between cycle length and respiration, and its lack of latency consistency with inhalation onset further complicates the use of LFPs as a precise marker of respiratory events. This band-specific variability reflects the multifaceted nature of OB activity, where different frequencies may be more or less sensitive to respiratory dynamics (Cleland and Borthakur, 2020; Kay, Lancaster, and Freeman, 1996).

Moreover, we observed differences in LFP-respiratory relationships between free-moving and head-fixed conditions. In general, free movement resulted in better performance of both time and frequency domain methods in predicting respiratory frequency. This suggests that the animal's behavioral state influences the quality of respiratory representation in LFPs, consistent with previous studies (Sterrett et al., 2024). However, the gamma envelope and respiratory cycle length correlation was stronger in head-fixed compared to free movement. Free movement likely introduces additional physiological variables, such as increased respiratory modulation or altered neural dynamics, which may differentially enhance or diminish the coupling between LFPs across multiple frequency bands and respiration.

Despite these challenges, our findings suggest that OB LFPs can still serve as useful proxies for respiratory frequency, especially when averaged across multiple sniff cycles. By using time-domain methods to detect peak-to-peak intervals in LFPs, we were able to infer sniff frequency with a relatively low error margin during free movement. However, the variability in LFP-respiratory delay renders the recovery of precise inhalation events more challenging. This difficulty underscores the limitations of LFPs in capturing fine-grained temporal dynamics of

respiration and highlights the need for complementary methods, such as thermistor-based sniff measurements, to accurately track respiratory events.

Future work should focus on refining models to account for the variability in LFP-respiratory coupling and explore ways to combine LFP-based methods with other non-invasive measures of respiration. Additionally, investigating the underlying neural mechanisms that contribute to the variability in LFP-respiratory alignment across different frequency bands and behavioral conditions may provide deeper insights into the relationship between respiration and OB neural activity.

In conclusion, while OB LFPs reliably track respiratory frequency, inferring precise inhalation timing remains a challenge due to the variability in LFP-respiratory delay. The use of time-domain methods shows promise in estimating respiratory frequency, particularly in free-moving conditions, but future work is needed to improve the temporal resolution of respiratory event detection from LFPs.

Conflict of interest

We declare we have no competing interests

Funding

NATIONAL INSTITUTE OF NEUROLOGICAL DISORDERS AND STROKE
Notice of Award
FAIN# R01NS123903

Acknowledgments

We thank James M. Murray, Avinash D. S. Bala and Morgan A. Brown for guidance, mentorship, and review of the manuscript.

Authors' contributions

Conceptualization, MS, SR, NH; Methodology, SR, NH; Formal Analysis, SR; Data Collection, TF; Resources, MS; Data Curation, SR; Writing—Original Draft, SR; Writing—Review & Editing, SR, MS, AS; Funding Acquisition, MS

References

Beshel, J., Kopell, N., & Kay, L. M. (2007). Olfactory bulb gamma oscillations are enhanced with task demands. The Journal of Neuroscience, 27(31), 8358–8365. https://doi.org/10.1523/jneurosci.1199-07.2007

Burton, S. D., Brown, A., Eiting, T. P., Youngstrom, I. A., Rust, T. C., Schmuker, M., & Wachowiak, M. (2022). Mapping odorant sensitivities reveals a sparse but structured representation of olfactory chemical space by sensory input to the mouse olfactory bulb. eLife, 11. https://doi.org/10.7554/elife.80470

Buzsáki, G., Anastassiou, C. A., & Koch, C. (2012). The origin of extracellular fields and currents — EEG, ECoG, LFP and spikes. Nature Reviews Neuroscience, 13(6), 407–420. https://doi.org/10.1038/nrn3241

Cleland, T. A., & Borthakur, A. (2020). A systematic framework for olfactory bulb signal transformations. Frontiers in Computational Neuroscience, 14. https://doi.org/10.3389/fncom.2020.579143

Cury, K. M., & Uchida, N. (2010). Robust odor coding via inhalation-coupled transient activity in the mammalian olfactory bulb. Neuron, 68(3), 570–585. https://doi.org/10.1016/j.neuron.2010.09.040

Fourcaud-Trocmé, N., Lefèvre, L., Garcia, S., Messaoudi, B., & Buonviso, N. (2019). High beta rhythm amplitude in olfactory learning signs a well-consolidated and non-flexible behavioral state. Scientific Reports, 9(1). https://doi.org/10.1038/s41598-019-56340-y

Grimaud, J., & Murthy, V. N. (2018). How to monitor breathing in laboratory rodents: A review of the current methods. Journal of Neurophysiology, 120(2), 624–632. https://doi.org/10.1152/jn.00708.2017

Gupta, P., Albeanu, D. F., & Bhalla, U. S. (2015). Olfactory bulb coding of odors, mixtures and sniffs is a linear sum of odor time profiles. Nature Neuroscience, 18(2), 272–281. https://doi.org/10.1038/nn.3913

Iwata, R., Kiyonari, H., & Imai, T. (2017). Mechanosensory-based phase coding of odor identity in the olfactory bulb. Neuron, 96(5). https://doi.org/10.1016/j.neuron.2017.11.008

Kay, L. M., Beshel, J., Brea, J., Martin, C., Rojas-Líbano, D., & Kopell, N. (2009). Olfactory oscillations: The what, how and what for. Trends in Neurosciences, 32(4), 207–214. https://doi.org/10.1016/j.tins.2008.11.008

Kay, L. M., Lancaster, L. R., & Freeman, W. J. (1996). Reafference and attractors in the olfactory system during odor recognition. International Journal of Neural Systems, 07(04), 489–495. https://doi.org/10.1142/s0129065796000476

Kleene, S. J. (2008). The electrochemical basis of odor transduction in vertebrate olfactory cilia. Chemical Senses, 33(9), 839–859. https://doi.org/10.1093/chemse/bjn048

Lim, R., Zavou, M. J., Milton, P.-L., Chan, S. T., Tan, J. L., Dickinson, H., Murphy, S. V., Jenkin, G., & Wallace, E. M. (2014). Measuring respiratory function in mice using unrestrained whole-body plethysmography. Journal of Visualized Experiments, (90). https://doi.org/10.3791/51755

Lockmann, A. L., Laplagne, D. A., & Tort, A. B. (2017). Olfactory bulb drives respiration-coupled beta oscillations in the rat hippocampus. European Journal of Neuroscience, 48(8), 2663–2673. https://doi.org/10.1111/ejn.13665

Losacco, J., Ramirez-Gordillo, D., Gilmer, J., & Restrepo, D. (2020). Learning improves decoding of odor identity with phase-referenced oscillations in the olfactory bulb. eLife, 9. https://doi.org/10.7554/elife.52583

Macrides, F., & Chorover, S. L. (1972). Olfactory bulb units: Activity correlated with inhalation cycles and odor quality. Science, 175(4017), 84–87. https://doi.org/10.1126/science.175.4017.84

McAfee, S. S., Ogg, M. C., Ross, J. M., Liu, Y., Fletcher, M. L., & Heck, D. H. (2016). Minimally invasive highly precise monitoring of respiratory rhythm in the mouse using an epithelial temperature probe. Journal of Neuroscience Methods, 263, 89–94. https://doi.org/10.1016/j.jneumeth.2016.02.007

Rinberg, D., Koulakov, A., & Gelperin, A. (2006). Sparse odor coding in awake behaving mice. The Journal of Neuroscience, 26(34), 8857–8865. https://doi.org/10.1523/jneurosci.0884-06.2006

Rojas-Li-bano, D., Frederick, D. E., EgaÃ±a, J. I., & Kay, L. M. (2014). The olfactory bulb theta rhythm follows all frequencies of diaphragmatic respiration in the freely behaving rat. Frontiers in Behavioral Neuroscience, 8. https://doi.org/10.3389/fnbeh.2014.00214

Shusterman, R., Smear, M. C., Koulakov, A. A., & Rinberg, D. (2011). Precise olfactory responses tile the sniff cycle. Nature Neuroscience, 14(8), 1039–1044. https://doi.org/10.1038/nn.2877

Spors, H., Wachowiak, M., Cohen, L. B., & Friedrich, R. W. (2006). Temporal dynamics and latency patterns of receptor neuron input to the olfactory bulb. The Journal of Neuroscience, 26(4), 1247–1259. https://doi.org/10.1523/jneurosci.3100-05.2006

Verhagen, J. V., Wesson, D. W., Netoff, T. I., White, J. A., & Wachowiak, M. (2007). Sniffing controls an adaptive filter of sensory input to the olfactory bulb. Nature Neuroscience, 10(5), 631–639. https://doi.org/10.1038/nn1892

Wachowiak, M. (2011). All in a sniff: Olfaction as a model for active sensing. Neuron, 71(6), 962–973. https://doi.org/10.1016/j.neuron.2011.08.030

Wilson, C. D., Serrano, G. O., Koulakov, A. A., & Rinberg, D. (2017). A primacy code for odor identity. Nature Communications, 8(1). https://doi.org/10.1038/s41467-017-01432-4